

**Research Article** 

# An Investigation of Driver Brake Pedal Stroke Input on Regenerated Braking Energy in Electric Vehicles via Dynamic Programming

## Nurettin Okan Çaycı1\*, Erkin Dinçmen2, İlyas İstif3

- <sup>1</sup> Amasya University, Tasova Yüksek Akin Vocational School, Motor Vehicles And Transportation Technologies Department, Railroad Construction Program, <a href="mailto:nurettin.cayci@amasya.edu.tr">nurettin.cayci@amasya.edu.tr</a>
  ORCID: <a href="https://orcid.org/0009-0002-0060-531X">https://orcid.org/0009-0002-0060-531X</a>
- <sup>2</sup> Yildiz Technical University, Control And Automation Engineering Department, <a href="mailto:erkin.dincmen@yildiz.edu.tr">erkin.dincmen@yildiz.edu.tr</a> ORCID: https://orcid.org/0000-0002-3234-281X
- <sup>3</sup> Yildiz Technical University, Mechanical Engineering Department, <u>istif@yildiz.edu.tr</u> ORCID: https://orcid.org/0000-0003-0792-249X

#### ARTICLE INFO

#### Article history:

Received 12 March 2025 Received in revised form 13 August 2025 Accepted 25 August 2025 Available online 30 September 2025

#### Keywords:

Fully electric vehicle, pedal stroke, regenerative braking, torque distribution, dynamic programming, energy efficiency

Doi: 10.24012/dumf.1655409

#### ABSTRACT

The rising popularity of electric vehicles increases the need for advanced techniques to improve driving efficiency. One such method is regenerative braking, which captures kinetic energy from the wheels—energy that would otherwise be lost as in traditional braking systems. In this study, a fully electric vehicle model which is three degrees of freedom was created with a fixed pedal-feel brake pedal and electric motors on both axles. The brake torque produced by pedal stroke input in different braking scenarios was allocated to the electric motors on the front and rear axles via dynamic programming in MATLAB/Simulink. It was compared to the case where the distribution ratio is fixed. More energy was gained with dynamic programming compared to the fixed allocation, and it is concluded that the duration of pressing the pedal and the repetition of pressing are effective parameters on energy recovery.

## Introduction

Growing concerns over environmental pollution and greenhouse gas emissions from fossil fuels have increased interest in electric vehicles. Additionally, fossil fuel reserves are finite, making alternative energy sources essential. Among these, electric cars stand out as the most viable option, partly due to their lack of noise pollution. However, challenges remain, such as limited battery energy density, short driving ranges, and long charging times. These issues highlight the need for maximizing battery efficiency, with regenerative braking playing a key role in energy conservation. Regenerative braking allows a DC motor to function as a generator, producing current that can recharge the battery. The efficiency of this process depends on several key factors, including the motor's torque and speed-dependent efficiency, battery internal resistance, open circuit voltage, temperature, charge level, and torque distribution between axles.

Studies in the literature on regenerative braking are as follows: Investigation [1] examined the self-reported behaviors of 36 Parisian drivers using an electric MINI E prototype for six months. The study found that EV operation requires a learning phase where drivers adapt to range limitations, establish charging routines, and modify trip planning habits. Work [2] developed a driver model to control vehicle speed and mimic human driving behavior. A regenerative braking strategy using a series brake system was implemented to replicate real-world braking performance. Analysis [3] focused on electric motor control strategies, including Sliding Mode, H2/H $\infty$ , Adaptive, and Fuzzy Logic Controllers, along with Artificial Neural Networks and Neuro-Fuzzy systems integrated with PID controllers. In contribution [4], an optimized braking force

<sup>\*</sup> Corresponding author

distribution approach was presented, maximizing regenerative energy recovery while ensuring braking efficiency by utilizing ground adhesion on both front and rear wheels. Research [5] performed a mathematical analysis of batteries and supercapacitors, evaluating their regenerative braking performance system characteristics using MATLAB/SIMULINK. The authors of [6] explored the feasibility of fully relying on regenerative braking for all deceleration scenarios, employing multiple generators with different gear ratios to achieve this goal. Publication [7] investigated control strategies for regenerative braking in electric vehicles powered by brushless DC motors, proposing and comparing two control methods. In [8] introduced a braking torque allocation strategy optimized with a particle swarm algorithm for an electro-hydraulic compound braking system in a dual-motor, dual-axle electric vehicle. Article [9] presented a new braking torque allocation strategy to inwheel motor EVs, prioritizing both safety and energy recovery. Model Predictive Control (MPC) was used to handle multi-objective constraints effectively. Paper [10] proposed a vehicle stability control system for a all-wheeldrive hybrid electric vehicle, optimizing braking torque distribution between regenerative braking and an electrohydraulic brake (EHB) using a genetic algorithm. Efforts in [11] focused on enhancing distributed torque control via Direct Torque Control (DTC) during regenerative braking. A Fuzzy Logic Controller for the BLDC motor was implemented and compared with a PI controller using MATLAB/Simulink. Research presented in [12] detailed the Energy-Optimal Deceleration Planning System (EDPS) for connected and autonomous EVs, utilizing a polynomial-based model to regenerative braking based on real-time driving data. Study [13] proposed a downshifting strategy based on clusterbased stochastic dynamic programming (SDP). The method categorized driving conditions using the K-means algorithm and modeled braking torque transitions with Markov chains. A support vector machine (SVM) enabled real-time application of SDP-based commands. In [14] developed a predictive control method integrating adaptive cubic exponential prediction and dynamic programming to enhance regenerative braking energy recovery. The model optimized motor braking torque and wheel cylinder pressures while considering electro-hydraulic braking dynamics. Lastly, work [15] examined the distribution of friction and electrical braking forces, introducing key parameters to evaluate braking energy recovery efficiency while ensuring vehicle safety under critical driving conditions.

In this study, depending on the driver's behavior, the distribution of the torque amount produced depending on the pedal stroke that occurs when the pedal is pressed and the pressing speed, which is the result of the change in the pedal stroke depending on time, to the electric motors located on the front and rear axles and also to the hydraulic brakes was done and regenerated energy into the battery was found in Matlab/Simulink environment via dynamic programming and Simulink model. Briefly, the effect of

pedal pressing behavior on the amount of regenerative energy was investigated.

#### **Electric Vehicle Model**

## Brake pedal model

Pedal stroke  $x_p$  pedal-dependent deceleration is utilized according to the fixed pedal feel [16]. The brake pedal displacement  $x_p$  and deceleration  $a_{dec}$  described as follow:

$$a_{dec} = \begin{cases} -(0.01x_p)g, & x_p \le 20mm \\ -(0.02x_p - 0.2)g, 20mm \le x_p \le 80mm \end{cases}$$
(1)

Total brake torque produced by pedal stroke  $T_b^{tot}$  is calculated as:

$$T_b^{tot} = m. \, a_{dec}. \, r_{eff} \tag{2}$$

where vehicle mass is m and wheel effective radius is  $r_{eff}$ .

### **Vehicle Dynamics**

The three-degree-of-freedom single track vehicle dynamics model is utilized in this paper. The longitudinal vehicle dynamics equation is given as follows:

$$ma_x = \sum F_x = F_{xf} cos \ \delta_f + F_{xr} - F_{yf} sin \ \delta_f \\ -F_g - F_{aero} - F_{roll}$$
 (3)

where, aerodynamic resistance is  $F_{aero}$ , rolling resistance is  $F_{roll}$ ,  $ma_x$  inertial resistance,  $F_g$  is the grade of the road and  $F_{xf}$ ,  $F_{xr}$  are the longitudinal and  $F_{yf}$ ,  $F_{yr}$  are the lateral forces on the front and rear wheels, respectively. Steering angle is denoted by  $\delta_f$ . The lateral vehicle dynamics is described as follows:

$$ma_v = \sum F_v = F_{xf} \sin \delta_f + F_{vf} \cos \delta_f + F_{vr}$$
 (4)

The yaw motion dynamics is given as follows:

$$I_z \dot{r} = (F_{xf} \sin \delta_f) l_f + (F_{yf} \cos \delta_f) l_f - F_{yr} l_r$$
 (5)

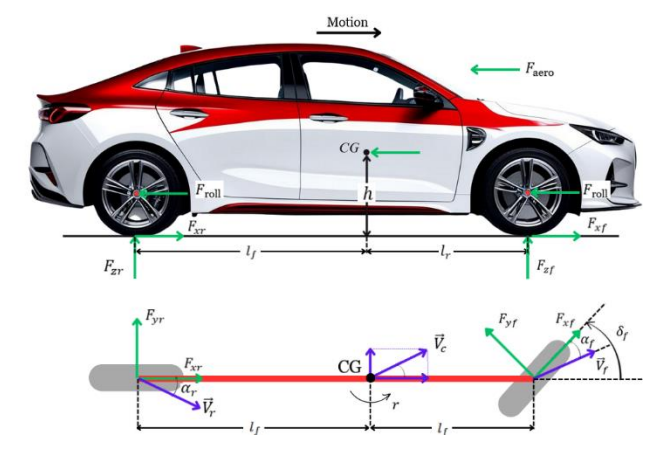


Figure 1. Distances, forces and angles.

I<sub>z</sub> is the vehicle inertia in yaw motion. Figure 1 displays the forces, angels and dimensions which is defined in equation

3, 4 and 5. Because lateral dynamics will be considered in future studies, the Simulink model created has three degrees of freedom. However, steering input was not provided in the braking scenarios covered in this article.

#### Tire Model

Dugoff tire model is utilized to compute tire forces. This model enables the calculation of forces considering both lateral and longitudinal force generation simultaneously [17]. As per the Dugoff model, the longitudinal forces of the front and rear tires are determined using equation (6).

$$F_{x(f,r)} = C_{x(f,r)} \frac{\sigma_{(f,r)}}{1 + \sigma_{(f,r)}} f(\lambda_{(f,r)})$$
 (6)

For the front and rear lateral tire forces, (7) is used,

$$F_{y(f,r)} = C_{\alpha(f,r)} \frac{\tan \alpha_{(f,r)}}{1 + \sigma_{(f,r)}} f(\lambda_{(f,r)})$$
 (7)

where,  $\sigma_f$  and  $\sigma_r$  represent the longitudinal slip ratios, while  $\alpha_f$  and  $\alpha_r$  denote the side slip angles of the front and rear tires, respectively. The cornering stiffness of the front and rear tires is denoted by  $C_{\alpha f}$  and  $C_{\alpha r}$ , whereas the longitudinal tire stiffness of the front and rear tires are represented as  $C_{x,f}$  and  $C_{x,r}$ . The values of  $f(\lambda_f)$  and  $f(\lambda_r)$  are determined using equations (8),  $\mu$  is tire-road friction coefficient.

$$f(\lambda_{(f,r)}) = \begin{cases} (2 - \lambda_{(f,r)}) \lambda_{(f,r)} & \text{when } \lambda_{(f,r)} < 1\\ 1 & \text{when } \lambda_{(f,r)} \ge 1 \end{cases}$$

$$\lambda_{(f,r)} = \frac{\mu F_{z(f,r)} (1 + \sigma_{(f,r)})}{2 \sqrt{(C_{x(f,r)}\sigma_{(f,r)})^2 + (C_{\alpha(f,r)}tan \ \alpha_{(f,r)})^2}}.$$
(8)

## **Braking Standards**

To guarantee vehicle braking safety, the UN/ECE has established specific regulations. As per the ECE R13-H brake standards, passenger cars must comply with defined brake force allocation criteria between the front and rear axles, [18]:

1. In all vehicle load conditions, the braking ratio is defined as the ratio of deceleration to gravitational acceleration, and when this ratio expressed by z is in the range  $z=0.15\sim0.8$ , the traction-use curve of the rear axle should not be greater than that of the front axle::

$$k_f \ge k_r \tag{9}$$

2. When the adhesion coefficient k is in the range of 0.2 ~ 0.8, the braking ratio must satisfy the following condition:

$$z \ge 0.1 + 0.7(k - 0.2) \tag{10}$$

If the values  $k = 0.15 \sim 0.8$  are substituted into inequality 10, respectively, the range of variation of z is found to be  $0.1 \le z \le 0.61$ . In this case, the adhesion coefficients of the front and rear wheels satisfy the following conditions:

$$k_f \le \frac{z + 0.04}{0.7} \tag{11}$$

$$k_r \le \frac{z + 0.04}{0.7} \tag{12}$$

where  $k_f$  and  $k_r$  are the theoretical adhesion coefficients on the front and rear axles, respectively, that is, the coefficients showing how effectively the wheels use road grip during braking, and they are calculated with the following formulas:

$$k_f = \frac{F_{x,f}}{F_{z,f}} = \frac{\beta zL}{l_r \cos(\alpha) + zh}$$
 (13)

$$k_r = \frac{F_{x,r}}{F_{z,r}} = \frac{(1-\beta)zL}{l_f \cos(\alpha) - zh}$$
 (14)

where;  $F_{z,f}$  and  $F_{z,r}$  are the normal forces acting on the front and rear axles from the road surface during braking, respectively,  $l_f$  is the distance between the front axle and the center of gravity (CG),  $l_r$  is the distance between the rear axle and the center of gravity, L is the total axle distance,  $\alpha$  is the road slope, h is the center of gravity height, and  $\beta$  is the braking torque allocation ratio.  $\beta$  is defined as follows:

$$\beta = \frac{T_f}{T_h^{tot}} \tag{15}$$

where  $T_f$  is the front axle torque. Substituting equations 13 and 14 into 9, 11 and 12 respectively, we obtain the following inequalities related to the torque allocation ratio:

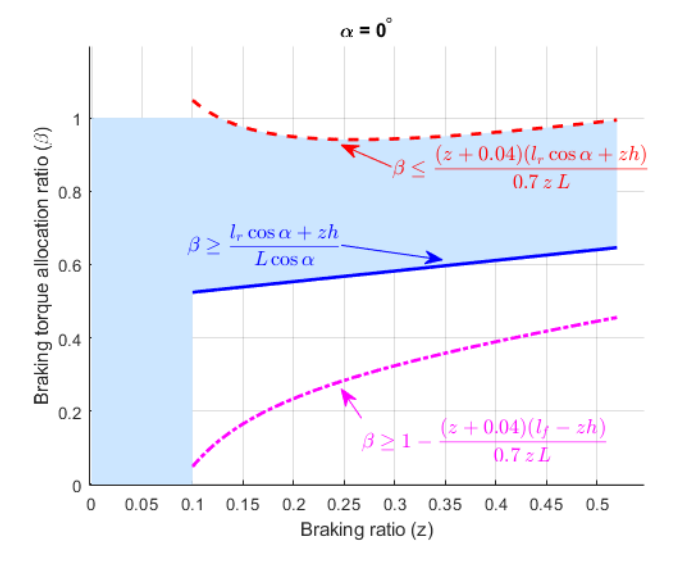


Figure 2.

The graph of the inequalities in (16),(17),(18) is plotted in figure (2). Under ECE regulations, the front wheels always maintain a higher adhesion coefficient than the rear wheels, ensuring braking stability. However, for optimal braking, the wheels' usage coefficients should remain below the road's adhesion coefficient  $(\mu)$ . Given the inequality in Equation 9, it is sufficient to ensure that only the front wheels' usage coefficient stays below  $\mu$ .

Table 1. Vehicle Parameters.

Symbol	Values
m	1623 kg
$l_f$	1.09 m
$l_r$	1.07 m
$\dot{h}$	0.627 m
$I_z$	$2166 \text{ kg.m}^2$
$r_{eff}$	0.327 m
Ĵ	$0.563 \text{ kg.m}^2$

$$\beta < \frac{\mu(zh + l_r)}{zL} \tag{19}$$

#### **Electrical Motor Model**

After determining the braking torque limits at both axles while accounting for the  $\beta$  value, the generated torques during braking, based on the pedal stroke, are utilized to compute the wheel's angular acceleration using the following equation:

$$\dot{\omega} = \frac{-T_b^{tot} - r_{eff} \left( m \cdot \alpha_x + F_{aero} + F_{roll} + F_g \right)}{I} \quad (20)$$

where *J* represents the wheel's inertia. Electric motor's efficiency is determined by using the efficiency map shown in Fig. 2. The power generated from both axles' EM as follows:

$$P_{EM,f} = T_b^{tot}.\beta \cdot \omega_{EM,f}.\eta_{EM,f}$$
 (21)

$$P_{EM,r} = T_b^{tot}.(1 - \beta) \cdot \omega_{EM,r}.\eta_{EM,r}$$
 (22)

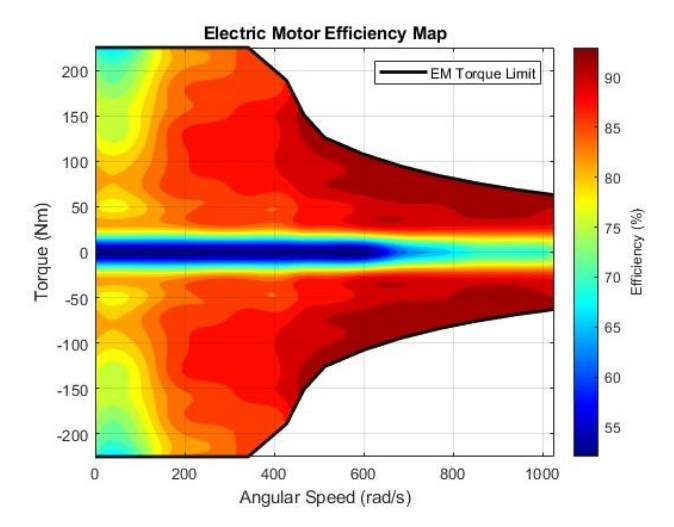


Figure 3. Electrical motor (EM) efficiency map

where  $\omega_{EM,f}$  and  $\omega_{EM,r}$  represent the angular speeds of the front and rear electric motors (EM), respectively, while  $\eta_{EM,f}$  and  $\eta_{EM,r}$  denote their efficiencies, as determined from the efficiency map in Figure 3. The total EM power, which can subsequently be used to determine the total energy stored in the battery, is calculated as follows:

$$P_{EM}^{tot} = P_{EM,f} + P_{EM,r} \tag{23}$$

### **Battery Model**

The equations necessary for calculating the power charged into the battery are given as follows [19]:

$$I_{chg} = \frac{-U_{oc} + \sqrt{Uoc^2 - 4R_{chg}P_{EM}^{tot}}}{2 * R_{chg}}$$
(24)

$$\eta_{bat} = U_{oc} / \left( U_{oc} + R_{chg} I_{chg} \right) \tag{25}$$

$$P_{hat} = \eta_{hat} P_{FM}^{tot} \tag{26}$$

here,  $U_{oc}$  represents the open-circuit voltage of the battery,  $R_{chg}$  is the battery's charging resistance,  $I_{chg}$  denotes the charging current,  $\eta_{bat}$  refers to the battery efficiency, and  $P_{bat}$  is the power stored in the battery.

# **Dynamic Programming**

Dynamic programming (DP) optimally distributes power by solving sequential sub-problems backward from the last to the first stage, significantly reducing calculations. However, since it requires prior knowledge of the entire driving scenario, it cannot be applied in real-time control. Instead, DP is used offline to evaluate the performance of instantaneous control algorithms. For the basic principle of the DP algorithm see also [20].

As observed, this process follows a backward calculation approach. In dynamic programming, this method requires fewer computations than forward one.

Where, 225×20 matrix is constructed for DP. The front axle (EM) torque levels are represented on the vertical axis, while the horizontal axis denotes the simulation time which is shown in Figure 4. The EM torque is segmented into 225 equal steps, ranging from zero to its maximum limit. The simulation runs with a step size of half second  $\Delta t$ , with braking concluding at  $T_{\rm end}$ , the 10th second, making the total duration 10 seconds.

 $\Delta t$  second before  $T_{end}$ , at the highest torque level, there are four possible transitions to the next state. These transitions are illustrated in Figure 4 with black arrows.

For instance, if the torque variation is restricted to a maximum of three levels owing to EM's response time, a change of four levels downward within  $\Delta t$  is not feasible.

Throughout this process, the amount of battery charge for each torque change is calculated. The optimal choice is the one that charges the battery the most.

$$J_{(Tend-1)}^{*}(1) = max \{ J_{(Tend-1)}^{Tend}(1,1), J_{(Tend-1)}^{Tend}(1,2), J_{(Tend-1)}^{Tend}(1,3), J_{(Tend-1)}^{Tend}(1,4) \}$$
(27)

The alternative torque levels after  $\Delta t$  second, corresponding to the second torque level, The procedure is described as follows:

$$J_{(Tend-1)}^{*}(2) = max \{J_{(Tend-1)}^{Tend}(2,1), J_{(Tend-1)}^{Tend}(2,2), J_{(Tend-1)}^{Tend}(2,3), J_{(Tend-1)}^{Tend}(2,4), J_{(Tend-1)}^{Tend}(2,5)\}$$
(28)

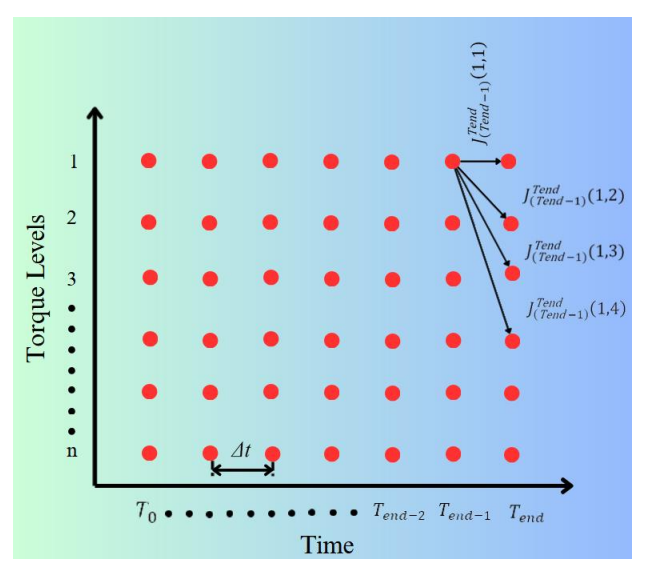


Figure 4. The first level alternatives of the DP.

Similarly, at the moment  $T_{\rm end}-2\Delta t$ , the possible alternatives are written, and calculations are then performed for the state transitions at  $T_{\rm end}-2\Delta t$  for the first torque level as follow:

$$J_{(\text{Tend}-2)}^{*}(1) = \max\{J_{\text{Tend}-2}^{\text{Tend}-1}(1,1) + J_{\text{Tend}-1}^{*}(1), J_{\text{Tend}-2}^{\text{Tend}-1}(1,2) + J_{\text{Tend}-1}^{*}(2), J_{\text{Tend}-2}^{\text{Tend}-1}(1,3) + J_{\text{Tend}-1}^{*}(3), J_{\text{Tend}-2}^{\text{Tend}-1}(1,4) + J_{\text{Tend}-1}^{*}(4)\}$$
(29)

This process continues backward through the time steps  $T_{\rm end}-3\Delta t$ ,  $T_{\rm end}-4\Delta t$ ,  $T_{\rm end}-5\Delta t$ ,  $T_{\rm end}-6\Delta t$  and so on. Upon completing the calculations, the torque distribution ratios that optimize battery charging during braking are found.

Meanwhile, rear EM's torque is calculated by using that  $T_r = T_b^{tot} - T_f$ . Using  $T_r$ , the power generated by the rear EM to charge the battery is calculated.

The flowchart of both the Simulink model and dynamic programming is given in Figure 5.

## **Simulation Study and Results**

Where three different braking scenarios of a vehicle traveling at a constant speed of 28 m/s in all scenarios were considered within 10 seconds. In the first scenario, the brake pedal is pressed slowly, the change in pedal stroke from zero to 30 mm and the torque amount generated accordingly are seen in Figure 6. The amount of energy recovered during braking is given in Figure 7. Accordingly, the continuous line represents the amount of energy gained via dynamic programming, while the amount of energy given with the dashed line represents the situation where  $\beta$  is constant. In both cases, the amount of energy gained when torque is shared with dynamic programming is greater than the

amount of energy gained when  $\beta$  is taken as constant. The maximum amount of energy gained in the situation where

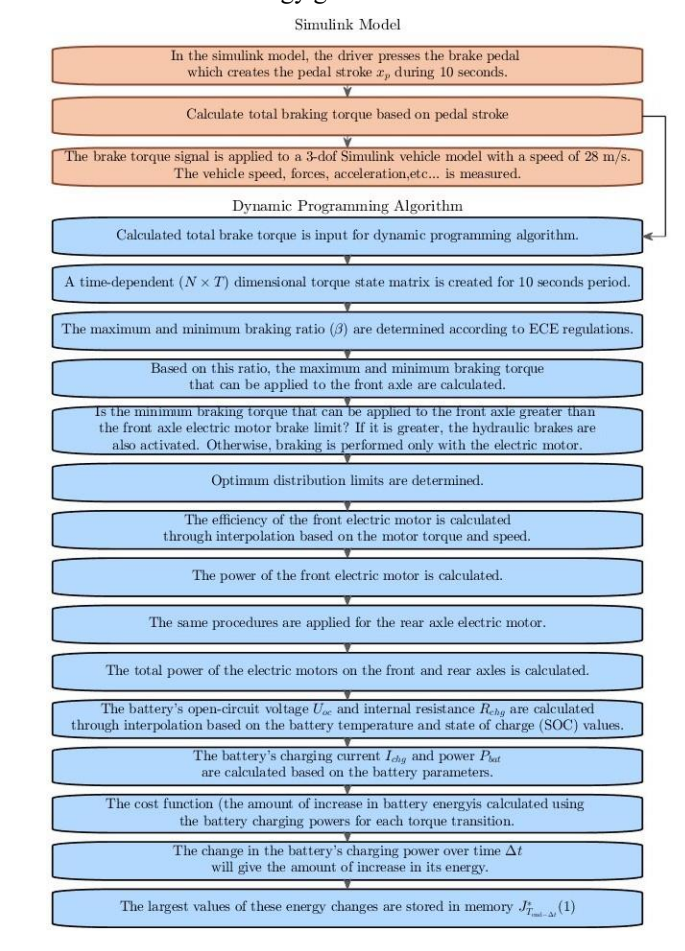


Figure 5. Flowchart.

 $\beta$  is constant is 570.334 kJ, and the amount of energy gained in dynamic programming is 586.952 kJ. In this scenario, 2.91% more gain was achieved with dynamic programming.

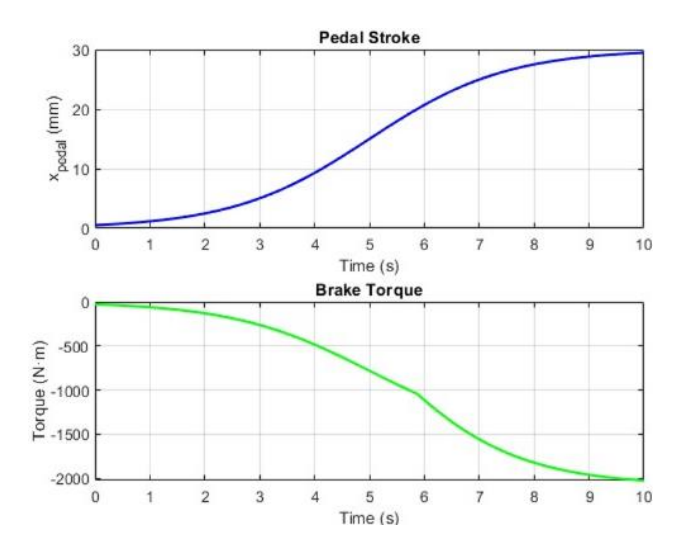


Figure 6. Change in pedal stroke with time and amount of torque generated for scenario 1

Figure 8 shows the graph of the time-dependent change of the pedal stroke applied in the second scenario and the torque amount generated accordingly. Here, the time-dependent change of the pedal stroke applied is greater than in the first scenario, and the pedal stroke is kept constant after the 6th second. Figure 9 shows the result of the amount of energy gained in this scenario. The maximum amount of energy gained in the case where  $\beta$  is constant is 580.442 kJ, and the amount of energy gained via dynamic programming is 598.995 kJ. This indicates that 3.196% more energy is gained thanks to dynamic programming.

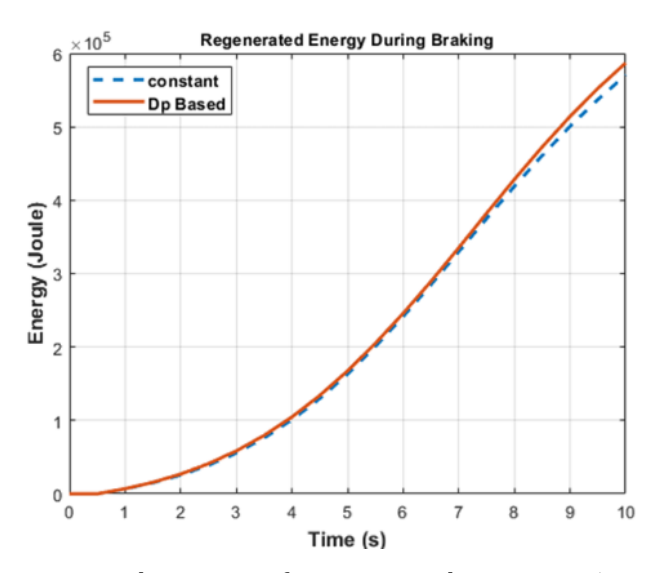


Figure 7. The amount of energy gained in scenario 1

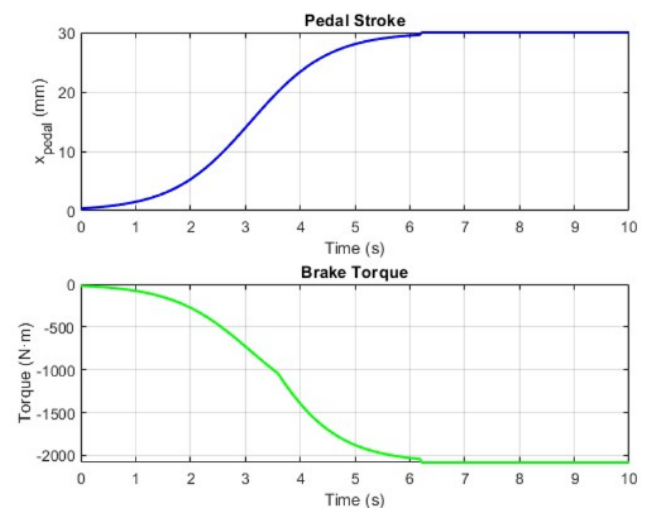


Figure 8. Pedal stroke and torque variation in ten sec. for scenario 2

Figure 10 shows the time-dependent change of the pedal stroke applied in the third scenario and the torque amount generated accordingly. The difference of the pedal stroke applied here from the previous two scenarios is that it considers the situation of pressing and releasing the pedal twice within a period of 10 seconds. Pressing the pedal takes longer than releasing the pedal. Figure 11 shows the result of the amount of energy gained in this scenario. The maximum amount of energy gained in the case where  $\beta$  is constant is 603.787 kJ, and the amount of energy gained in

dynamic programming is 621.935 kJ. This indicates that there is 3% more energy gain in terms of dynamic programming.

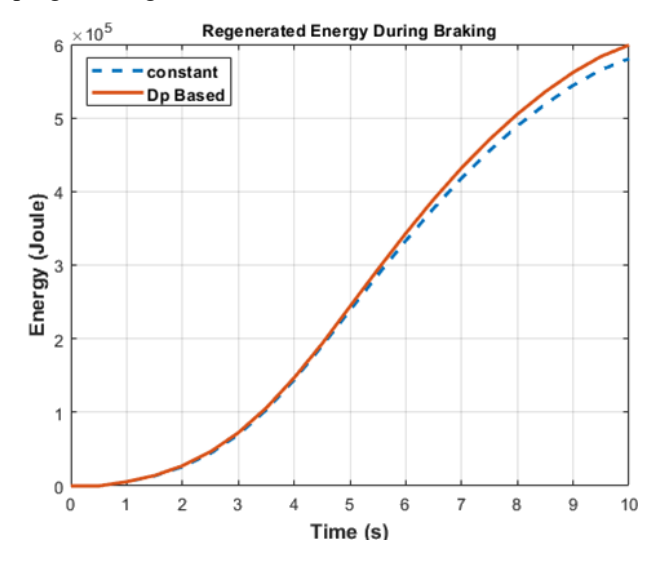


Figure 9. The amount of energy gained in scenario 2

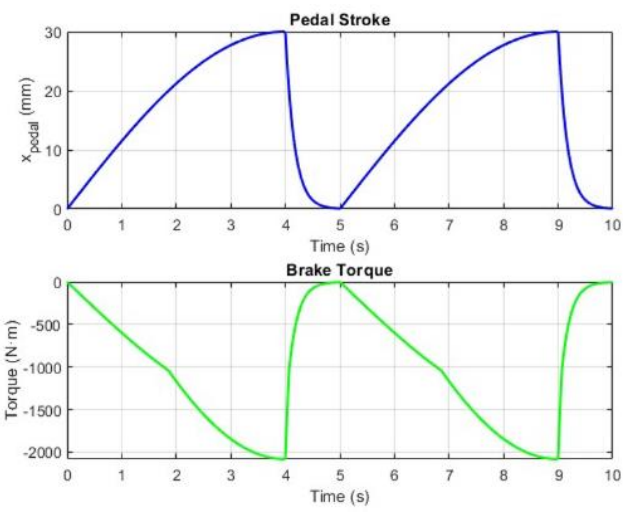


Figure 10. Pedal stroke and torque variation in ten sec. for scenario 3

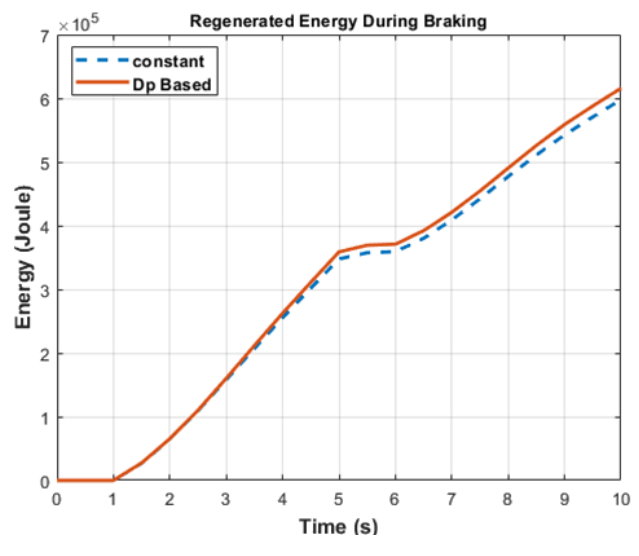


Figure 11. The amount of energy gained in scenario 3

Table 2. Results.

Scenarios	Regenerated Energy via DP (kWh)	Regenerated Energy by constant $\beta$ (kWh)	Gain (%)
1	0.163	0.158	2.91
2	0.166	0.161	3.196
3	0.173	0.168	3

In all 3 simulations, the energy amounts gained via dynamic programming provide approximately 3% more gain than the energy gains in cases where  $\beta$  is constant. In addition, the pedal stroke is taken as 30 mm in all 3 simulations. As seen in the graph in Figure 10, the highest total energy is obtained in the third scenario. The change in vehicle speed in 10 seconds is given in Figure 10. Since the vehicle speed does not drop to zero in a braking as in scenario 1, the total energy gained is lower than in scenario 2. However, if the simulation period is extended and the brake is applied to reduce the speed to zero, it is certain that the amount of energy gained in scenario 1 will exceed scenario 2. The real gain here is in scenario 3. As a result, there is more energy gain in pressing and releasing the brake. In Table 2, the amount of energy gained is given in kWh.

#### Conclusion

Dynamic programming provides 3% approximately more energy recovery than using a constant  $\beta$  in all braking scenarios. The highest energy gain occurs in the third scenario with variable pedal application, showing that press-release braking is more efficient for regenerative systems. It appears that pedal behavior is crucial for energy recovery. Future studies could include a frequency that maximizes energy recovery after determining the braking torque requirement and yaw motion could be taken in to account. In addition, the data obtained here will be used to train artificial neural network and the torque distribution process will be undertaken by it.

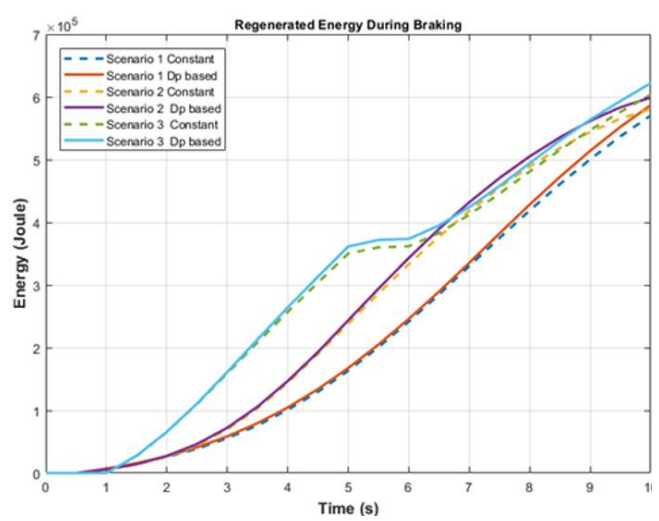


Figure 12. The amount of energy gained for all scenarios

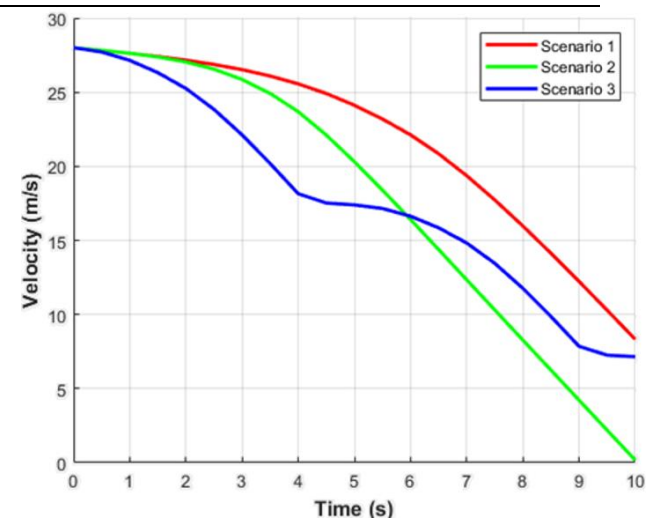


Figure 13. Velocities for all scenarios

# Aknowledgement

The authors extend their heartfelt gratitude to the Turkish National Research Council (TUBITAK) for its generous support under grant no: 122M994.

## References

- [1] E. Labeye, M. Hugot, C. Brusque, and M. A. Regan, "The electric vehicle: A new driving experience involving specific skills and rules, "Transportation Research Part F: Traffic Psychology and Behaviour", vol. 37, pp. 27–40, Feb. 2016.
- [2] Miri, I., Fotouhi, A., and Ewin, N., "Electric vehicle energy consumption modelling and estimation—A case study," International Journal of Energy Research, vol. 45, no. 1, pp. 501-520, Jan. 2021.
- [3] G. A. Chandak and A. A. Bhole, "A review on regenerative braking in electric vehicle," 2017 Innovations in Power and Advanced Computing Technologies (i-PACT), pp. 1-5, 2017.
- [4] J. Zhiming, R. Dianbo, S. Baoyu, C. Shumei, and S. Gang, "The research of regenerative braking control strategy for advanced braking force distribution," in 2009 Fifth International Conference on Natural Computation, vol. 6, Aug. 2009, pp. 458–462. IEEE
- [5] Bogineni, J., & Nakka, J. (2022, January). Battery and supercapacitor performance analysis during regenerative braking in electric vehicles. In 2022 International Conference on Computing,

- Communication and Power Technology (IC3P) (pp. 108-112). IEEE.
- [6] W. J. Melis and O. Chishty, "Fully regenerative braking and improved acceleration for electrical vehicles," Int. J. Sustain. Energy Dev. (IJSED), vol. 2, no. 1, pp. 75– 80, 2013.
- [7] P. S. Shenil, "Novel regenerative braking controllers for electric vehicle driven by BLDC motor," in 2021 Fourth International Conference on Electrical, Computer and Communication Technologies (ICECCT), 2021.
- [8] W. Jiang, R. Zheng, G. Zhang, Z. Zhu, W. Wang, C. Li, and Q. Tong, "Optimal torque distribution strategy for electric vehicles with electro-hydraulic compound braking system," in 2023 7th CAA International Conference on Vehicular Control and Intelligence (CVCI), Oct. 2023, pp. 1–6. IEEE.
- [9] W. Xu, H. Chen, H. Zhao, and B. Ren, "Torque optimization control for electric vehicles with four inwheel motors equipped with regenerative braking system," Mechatronics, vol. 57, pp. 95–108, 2019.
- [10] D. H. Kim, J. M. Kim, S. H. Hwang, and H. S. Kim, "Optimal brake torque distribution for a four-wheeldrive hybrid electric vehicle stability enhancement," Proc. Inst. Mech. Eng., Part D: J. Automob. Eng., vol. 221, no. 11, pp. 1357–1366, 2007.
- [11] G. BhaskarRao, N. Mounika, K. Chandana, A. DileepKumar, G. AshokBabu, and S. HimaVarshini, "Control strategy for regenerative braking in electric vehicles," International Journal of Scientific Research in Engineering and Management, 2023, doi: 10.55041/ijsrem18484
- [12] D. Kim, J. SooEo, and K.-K. K. Kim, "Parameterized energy-optimal regenerative braking strategy for connected and autonomous electrified vehicles: A realtime dynamic programming approach," *IEEE Access*, 2021. DOI: 10.1109/access.2021.3098807
- [13] B. Liu, L. Li, X. Wang, and S. Cheng, "Hybrid electric vehicle downshifting strategy based on stochastic dynamic programming during regenerative braking process," IEEE Transactions on Vehicular Technology, 2018. [Online]. Available: DOI: 10.1109/TVT.2018.2815518.
- [14] J. Zhang, Y. Yang, D. Qin, C. Fu, and Z. Cong, "Regenerative braking control method based on predictive optimization for four-wheel drive pure electric vehicle," IEEE Access, vol. 9, pp. 1-10, 2021. DOI: 10.1109/ACCESS.2020.3046853.
- [15] C. Qiu, G. Wang, M. Meng, and Y. Shen, "A novel control strategy of regenerative braking system for electric vehicles under safety critical driving situations," Energy, vol. 149, pp. 329–340, Apr. 2018, doi:10.1016/j.energy.2018.02.046.
- [16] U. Caliskan and V. Patoglu, "Efficacy of haptic pedal feel compensation on driving with regenerative

- braking," IEEE Transactions on Haptics, vol. 13, no. 1, pp. 175-182, 2020.
- [17] Rajamani, R.: Vehicle Dynamics and Control. Springer, New York (2012)
- [18] Regulation No 13 of the Economic Commission for Europe of the United Nations (UN/ECE) Uniform provisions concerning the approval of vehicles of categories M, N and O regarding braking, (OJ L 257 30.9.2010, p. 1) [Online]. Available: https://op.europa.eu/s/y1QM
- [19] E. Dincmen, B. Güvenç, "A control strategy for parallel hybrid electric vehicles based on extremum seeking," Vehicle System Dynamics, vol. 50, pp. 199-227, 2012, doi: 10.1080/00423114.2011.577224.
- [20] O. Ergun, N. O. Cayci, E. Dincmen, and I. Istif, "Optimum torque distribution during regenerative braking in a fully electrical vehicle via dynamic
- [21] programming," in 2023 7th International Symposium on Multidisciplinary Studies and Innovative Technologies (ISMSIT), Oct. 2023, pp. 1-6.

## Appendix A

#### Nomenclature

Symbol	Description
α	Road slope angle (rad)
$a_{ m dec}$	Pedal-dependent vehicle deceleration
$a_x$	Longitudinal acceleration ( m/s <sup>2</sup> )
$a_y$	Lateral acceleration (m/s <sup>2</sup> )
$\alpha_{(f,r)}$	Side slip angle (front/rear)
β	Braking torque distribution ratio
$C_{\alpha(f,r)}$	Cornering stiffness (front/rear tires)
$C_{x(f,r)}$	Longitudinal stiffness (front/rear tires)
$F_{ m aero}$	Aerodynamic drag force
$f(\lambda_{(f,r)})$	Dugoff friction function
$F_g$	Gravitational force due to road slope
$F_{ m roll}$	Rolling resistance force
$F_{xf}$ , $F_{xr}$	Longitudinal tire forces (front/rear)
$F_{yf}$ , $F_{yr}$	Lateral tire forces (front/rear)
$F_{z(f,r)}$	Normal force on front/rear tires
h	Height of CG from ground (m)
$I_{ m chg}$	Battery charging current (A)

$I_z$	Yaw moment of inertia of vehicle ( $kg \cdot m^2$ )
J	Wheel inertia ( $kg \cdot m^2$ )
$k_f, k_r$	Adhesion utilization coefficient (front/rear)
L	Wheelbase (distance between axles) (m)
$l_f$	Distance from CG to front axle (m)
$l_r$	Distance from CG to rear axle (m)
m	Vehicle mass (kg)
$\mu$	Tire-road friction coefficient
$\eta_{ m bat}$	Battery charging etticiency
$\eta_{EM(f,r)}$	Efficiency of front/rear electric motor
$P_{\rm bat}$	Power charged into the battery
$P_{EM(f,r)}$	Power generated from front/rear electric motor
$P_{EM}^{tot}$	Total power generated by electric motors
r	Yaw rate (rad/s)
$r_{eff}$	Effective wheel radius (m)
$R_{\rm chg}$	Internal resistance during charging $(\Omega)$
$\sigma_{(f,r)}$	Longitudinal slip ratio (front/rear)
$T_b^{ m tot}$	Total brake torque generated by the pedal stroke
$U_{oc}$	Open-circuit voltage of battery (V)
$\delta_f$	Front wheel steering angle (rad)
$\omega_{EM(f,r)}$	Angular speed of front/rear electric motor (rad/s)
$\dot{\omega}$	Angular acceleration of wheel (rad/s <sup>2</sup> )
$x_p$	Brake pedal stroke (mm)
Z	Braking intensity (deceleration/gravity)
$ec{V}_f$	Front axle velocity (m/s)
$ec{V}_r$	Rear axle velocity (m/s)
$ec{V}_c$	Velocity of the CG (m/s)
$\lambda_{(f,r)}$	Combined slip function (front/rear)
CG	Center of gravity